Available online at www.sciencedirect.com

ScienceDirect

IFAC PapersOnline CONFERENCE PAPER ARCHIVE

IFAC PapersOnLine 56-2 (2023) 4252–4257

Data-driven Temperature Estimation for a Multi-Stage Press Hardening Process

Malte Wrobel * **Juri Martschin** ** **Thomas Meurer** *
Erman Tekkaya **

* *Digital Process Engineering Group, Institute for Mechanical Process Engineering and Mechanics, Karlsruhe Institute of Technology (KIT), 76187 Karlsruhe, Germany (e-mail: {malte.wrobel,thomas.meurer}@kit.edu)*
** *Institute of Forming Technology and Lightweight Components, Dortmund University, 44227 Dortmund, Germany (e-mail: {juri.martschin,erman.tekkaya}@iul.tu-dortmund.de)*

Abstract: In a multi-stage press hardening process with a sheet material in a progressive die the material is first rapidly austenitized, pre-cooled, stretch-formed, and finally die bent. The product properties result from the thermo-mechanical history. With the aim to estimate and subsequently to directly control these properties a data-driven estimation of the spatial-temporal temperature distribution in the sheet is developed in this work. Therefore a data-driven dynamical model is designed via the Dynamic Mode Decomposition (DMD) using a Finite Element (FE) simulation as data basis. This model is extended to a parameter-dependent formulation (parametric DMD) capturing the process parameters stroke rate, blank holder force, and austenitization temperature, which serve as inputs to the model. The approach is verified by a comparison of the data-driven model with the original FE model. To estimate the temperature distribution a discrete time system representation is formulated, where the stage dependent and hence time varying output matrix is constructed for thermocouples integrated into the individual stages. Based on this a Kalman filter is designed and evaluated in simulation.

Keywords: Dynamic Mode Decomposition, Finite Element Method, Model Order Reduction, Metal Sheet Forming, Software Sensor, Observers, Temperature Estimation

1. INTRODUCTION

Large batch sizes of geometrically complex, hardened components can be produced by press hardening of sheet metal in multi-stage dies. Examples include the hot shearing and hardening of automotive belt buckles (Mori et al. (2017a)) and transmission parts (Mori et al. (2017b)). Even in single-stage press hardening, the thermal and mechanical interactions and thus the resulting product properties are difficult to predict. In the case of multi-stage press hardening, the modeling effort to determine a functional process window increases considerably. Furthermore in case of multi-stage press hardening, greater uncertainties in the prediction of the product properties are given by a multi-stage error propagation and an extended perturbation collective. To compensate for the uncertainties and thus to implement a robust and adaptable production, forming processes can be operated in a closed control loop (Allwood et al. (2016)). The overall goal of this project is to implement a comprehensive property control, i.e., a multivariable control, in a multi-stage press hardening.

This is complicated by the fact that online measurements of properties such as hardness in press hardening are currently only possible to a limited extent in the running process. To address this, the present work considers the development of a data-driven temperature estimation scheme for the real-time reconstruction of the spatial-temporal temperature distribution in the workpiece. Knowledge of the temperature profile allows to predict the final microstructure, which is a preliminary for the realization of property-controlled multi-stage press hardening. In this context Kloeser et al. (2021) proposed a temperature estimator design based on the Proper Orthogonal Decompostion (POD) applied to a high-order Finite Element (FE) approximation of the process. Differing from this the present work uses a data-driven approach to determine a reduced order mathematical process model (Kutz et al., 2016). For the actual evaluation the Dynamic Mode Decomposition (DMD) is applied and extended to the present process characteristics using high-dimensional data generated from a detailed process simulation using the FE code `LSDyna`. Applications of DMD are numerous covering, e.g., fluid dynamics (Schmid, 2010), power systems (Barocio et al., 2014), and trading strategies (Mann and Kutz, 2016). Several extensions to the classical DMD exist involving in particular the DMD with control (DMDc) to handle known and unknown input operators (Proctor et al., 2016). The input-output DMD (ioDMD) additionally takes input and output data into account for the modeling process (Benner et al., 2018).

Differing from the summarized applications and techniques the considered multi-stage press hardening process is characterized by operator-defined process parameters such as

10.1016/j.ifacol.2023.10.1785

stroke rate or dwell time that can be changed only at certain operating times but not continuously over time. These, however, have to be included into a control concept addressing the evolution of the product properties. To address this a parametric DMD similar to Sayadi et al. (2015) is considered, where the data of different simulations for individual parameter sets are stacked. This resembles the so-called multi-domain DMD for a phase-consistent model from multiple overlapping spatial domains (Nair et al., 2020). To be able to switch between different process parameters in the resulting reduced order model Lagrangian interpolation is used. The resulting DMD-based model is used to design a state estimator to determine the spatial-temporal temperature distribution in the workpiece. Due to the sensor configuration with different sensor setups in the individual stages a time varying output matrix is introduced to capture the movement and processing of the workpiece(s) through the subsequent stages.

The paper is structured as follows. The multi-stage press hardening process is described in Section 2. The data-driven reduced system model generated using stacking and parametric DMD is developed in Section 3. Section 4 addresses the design and the evaluation of a Kalman filter based on the reduced order model with time varying output matrix. Some final remarks are given in Section 5.

2. PROCESS DESCRIPTION

The overall objective is to control the product properties based on the microstructure such as the distribution of hardness, while simultaneously maintaining a desired product geometry during a multi-stage press hardening process. For developing such a multivariable closed-loop control, multi-stage press hardening in a progressive die operated in a servo press having the stage sequence presented in Fig. 1 is considered. The material used for this forming process is the press hardening steel 22MnB5, with its microstructure evolution having a pronounced sensitivity towards the thermo-mechanical treatment during the multi-stage process. When this steel is quenched at cooling rates greater than the critical cooling rate $r_{c,crit}$ after austenitizing, the final microstructure of the selected material becomes almost completely martensitic. At lower cooling rates ($r_c < r_{c,crit}$) a mixed microstructure with lower hardness is formed. Furthermore, the critical cooling rate for achieving a martensitic microstructure increases with strain imposed by forming the 22MnB5 sheet material in the austenitic state. The material to be processed with the progressive die having initially a ferritic-pearlitic microstructure is in the form of slit strip with a sheet thickness $s = 2\,\text{mm}$ and a strip width of 200 mm.

During preliminary stages (not shown in Fig. 1) the slit strip is precut at room temperature into rectangular blanks ($w \times l = 60 \times 140\,\text{mm}$), which are linked to each other by a strip connection for the transfer through the tool stages. In the first control-relevant die stage, the precut rectangular blanks are heated to the austenitizing temperature T_γ by an induction coil. In the pre-cooling stage, a temperature profile is set along the longitudinal direction of the blank using resistance heating and cooling with compressed air from flat fan nozzles. Hereby it is aimed to tailor the phase transformation by the temperature-dependent flow of the material in the subsequent forming

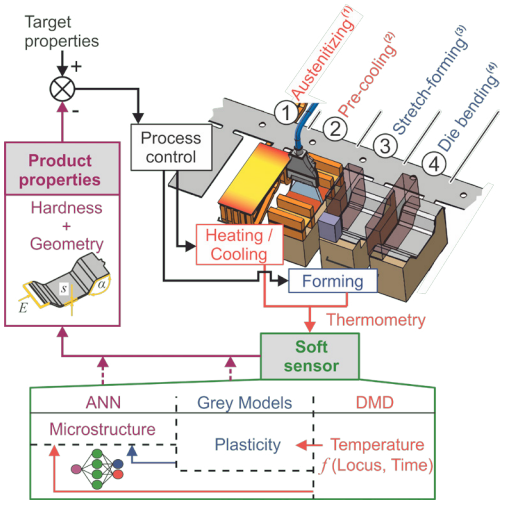

(a) Control loop including all process stages.

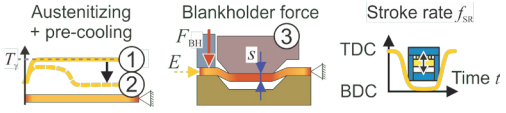

(b) Impacts of control variables T_γ, F_{BH}, and f_{SR}.

Fig. 1. Schematics of multi-stage press hardening process.

stages as well as the thermal history. In the stretch drawing stage, a hat shaped profile is formed. The blankholder force F_{BH} can be adjusted during stretch drawing, which allows the sheet draw-in E and thus also the sheet thinning Δs to be set. Finally, during die bending, a side wall of the previously formed hat shaped profile is bent and the final geometry is calibrated by completing the quenching in the closed die. By adjusting the stroke rate f_{SR} of the press, the contact time of the tools with the hot sheet can be adjusted, which allows to vary the average cooling rate during the multi-stage process.

For a reconstruction of the product properties with a soft sensor cascade the temperature is measured locally with five spring loaded thermocouples installed in the die stages while the ram is near the bottom dead center. In addition, the temperature distribution is observed with a thermal imaging camera and measured locally with pyrometers. Based on these measurements, the spatial-temporal temperature distribution is determined using the estimator developed in Section 4 utilizing the DMD model derived in Section 3. This distribution provides the baseline for calculating the plasticity and thus the geometry using suitable grey-box models and predicting the hardness by a artificial neuronal network. The resulting values are then compared with the target value to adjust the input variables (T_γ, F_{BH}, f_{SR}) accordingly.

3. DATA-BASED MODEL GENERATION

In the following the model generation using stacking and parametric DMD is described making use of simulation data from a detailed FE simulation.

3.1 High fidelty model

To determine the temperature distribution $\boldsymbol{T}_{\text{Sim}}(x,t)$ in the sheet during the tool stages of the progressive die,

the multi-stage process is simulated with the FE code `LSDyna` (solver: R12.0.0). The basic structure for modeling each of the process stages follows the setup described in Hochholdinger (2012). Heat exchange between sheet, tools and the environment as well as the flow stress and Young's modulus of the 22MnB5 sheet material are modeled with values based on Shapiro (2009). The tools are meshed with rigid and the blank with elasto-viscoplastic 12 node thermal thick shells, whereby the heat flow in the sheet thickness direction can be accounted for. The meshed blank is shown in Fig. 2. The spatial positions of the nodes change over time as seen in the difference between the start of the forming process in Fig. 2(a) and the end in Fig. 2(b). Gray nodes serve as positions for fixture elements and are not relevant for the forming process. The red and green nodes are relevant to the forming process. For reasons of simplicity only the temperatures of the green nodes are simulated as the temperatures do not change significantly in x-direction. The microstructure evolution governed by the diffusionless phase transformation from austenite to martensite and the phase transformation by diffusion from austenite to bainite, ferrite or pearlite is modelled with the material model Mat248 based on Hippchen et al. (2016). A strain dependent scaling of the activation energy for phase transformation is used to cover the effect of forming the 22MnB5 in the austenitic state on microstructure evolution as proposed by Bambach et al. (2017). The inductive heating of the blank in the austenitizing stage is not simulated. Before the transfer to the pre-cooling stage, a fully austenitized blank with a defined temperature distribution is assumed. Also, the resistance heating as well as the cooling by compressed air in the pre-cooling stage is taken into account in a simplified way by a thermal boundary condition imposed on the nodes of the sheet.

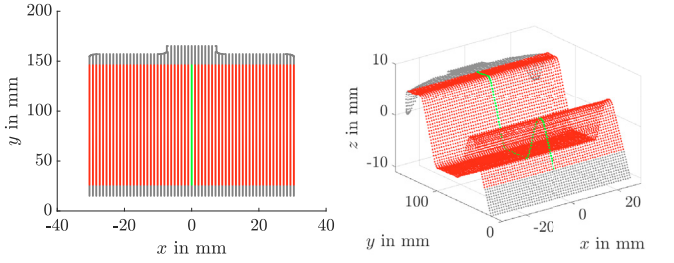

(a) 2D-Mesh at the start of the forming process.

(b) 3D-Mesh at the end of the forming process.

Fig. 2. Blank mesh evolution during the forming process.

3.2 Dynamic Mode Decomposition

The DMD is a model order reduction (MOR) technique to isolate spatially coherent modes each associated with a fixed frequency. DMD provides not only modes, but also enables to determine a linear model for the temporal evolution of the modes. The actual evaluation makes use of either measured or simulated data summarized in the data vector $\boldsymbol{T}_{\mathrm{Sim}}(t_k)$ collected at discrete times $t_k = (k-1)\Delta t$, $k = 1, 2, \dots m$. In the considered scenario $\boldsymbol{T}_{\mathrm{Sim}}(t_k)$, $k = 1, 2, \dots m$ denote the sampled temperatures obtained from the detailed `LSDyna` simulation at all $n = 119$ relevant (green marked) nodes of the sheet metal (cf. Fig. 2) passing the three consecutive processing stages 2, 3 and 4 of Fig. 1.

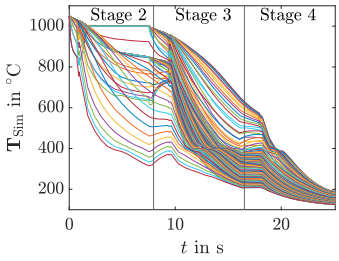

Fig. 3. Temperature evolution over the 3 simulated stages.

Hence, a Lagrangian perspective is taken. Fig. 3 shows the time evolution of $\boldsymbol{T}_{\mathrm{Sim}}$. Let

$$X_1 = \left[\boldsymbol{T}_{\mathrm{Sim}}(t_0)\ \boldsymbol{T}_{\mathrm{Sim}}(t_1)\ \dots\ \boldsymbol{T}_{\mathrm{Sim}}(t_{m-2})\right] \in \mathbb{R}^{n\times(m-1)}$$
$$X_2 = \left[\boldsymbol{T}_{\mathrm{Sim}}(t_1)\ \boldsymbol{T}_{\mathrm{Sim}}(t_2)\ \dots\ \boldsymbol{T}_{\mathrm{Sim}}(t_{m-1})\right] \in \mathbb{R}^{n\times(m-1)}$$

denote the snapshot matrices. The number of time steps $m = t_e/\Delta t$ depend on the process time t_e and the sampling time Δt. DMD starts from the assumption that $\boldsymbol{T}_{\mathrm{Sim}}(t_k)$ and $\boldsymbol{T}_{\mathrm{Sim}}(t_{k+1})$ are approximately related by a linear operator $A \in \mathbb{R}^{n\times n}$ according to $\boldsymbol{T}(t_{k+1}) \approx A\boldsymbol{T}(t_k)$ with the DMD state vector $\boldsymbol{T}(t_k)$. In view of the snapshot matrices this is equivalent to $X_2 \approx AX_1$. A least-squares solution A is obtained by minimizing the Frobenius norm of $\|X_2 - AX_1\|$, which yields $A = X_2X_1^\dagger$ with $X_1^\dagger$ the pseudoinverse of X_1. The singular value decomposition (SVD) provides an efficient way to compute $X_1^\dagger$. Moreover, this also allows to determine a reduced order representation A_r of A. The rank-r truncated DMD is computed as follows.

(i) For X_1 the rank-r truncated SVD $X_1 \approx U_rS_rV_r^*$ with $U_r \in \mathbb{C}^{n\times r}$, $S_r \in \mathbb{C}^{r\times r}$ and $V_r \in \mathbb{C}^{m\times r}$ is evaluated, where $\cdot^*$ denotes the complex conjugate transpose.

(ii) The matrix A can be determined from the SVD using

$$A = X_2X_1^\dagger \approx X_2V_rS_r^{-1}U_r^* = \bar{A}.$$

Hence, $\boldsymbol{T}(t_{k+1}) = \bar{A}\boldsymbol{T}(t_k)$ is obtained to approximate the evolution of the data (state) vectors. To reduce the system order, the linear transformation $\boldsymbol{T}_r(\cdot) = U_r^*\boldsymbol{T}(\cdot)$ and thus $\boldsymbol{T}(\cdot) \approx U_r\boldsymbol{T}_r(\cdot)$ with $\boldsymbol{T}_r \in \mathbb{R}^r$ for $r \ll n$ is introduced to obtain

$$\boldsymbol{T}_r(t_{k+1}) = A_r\boldsymbol{T}_r(t_k) \tag{1}$$

with $A_r = U_r^*\bar{A}U_r = U_r^*X_2V_rS_r^{-1}$.

(iii) The eigendecomposition of A_r is computed from $A_rW = W\Lambda$. The eigenvalues of $\bar{A}$ are summarized in the diagonal matrix Λ and the related eigenvectors, the DMD modes, are given by the columns of $\Phi = X_2V_rS^{-1}W$.

Transforming the discrete time eigenvalues λ_k to continuous time using $\omega_k = \ln(\lambda_k)/\Delta t$ (Kutz et al., 2016), the approximate solution of (1) for time t is given by

$$\boldsymbol{T}(t) \approx \Phi e^{\Omega t}\boldsymbol{b} \tag{2}$$

with the DMD modes Φ and the diagonal matrix Ω with eigenvalues ω_k. The vector $\boldsymbol{b} = \Phi^\dagger\boldsymbol{T}(0)$ is calculated using the initial condition $\boldsymbol{T}(0) = \Phi\boldsymbol{b}$.

The sampling time $\Delta t = 0.01\,\mathrm{s}$ and truncation order $r = 50$ are chosen to ensure the numerical stability of the reduced order system, see, e.g., Mamakoukas et al. (2020). The results depicted in Fig. 4 are achieved by simulating the approximate solution (2). The blue line shows the

evolution of the mean temperature $\text{mean}(\boldsymbol{T}) = \sum_{i=1}^{n} T_i/n$ over time. The colored bars visualize the difference between the DMD model and the corresponding `LSDyna` simulation $\Delta\boldsymbol{T} = \|\boldsymbol{T} - \boldsymbol{T}_{\text{Sim}}\|_1$. The grey bars show the maximum difference denoted by $\max(\Delta\boldsymbol{T})$ at a node and the red bars visualize the mean difference $\text{mean}(\Delta\boldsymbol{T}) = \sum_{i=1}^{n} \Delta T_i/n$ over all nodes. It becomes apparent that the difference $\Delta\boldsymbol{T}$ between DMD and full model is small with slightly larger values at the transition point between two stages. In particular, the average difference over all nodes takes a maximum value of 10 °C at the stage transitions and the maximum difference of all nodes behaves in a similar way with higher values of up to 40 °C.

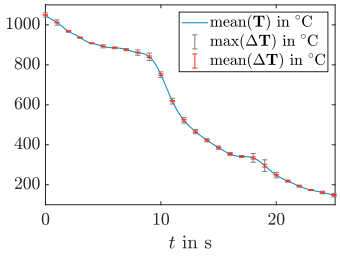

Fig. 4. Comparison of temperature evolution between the solution (2) of the reduced order DMD model (1) and the full order `LSDyna` simulation.

In view of the real-time application of the reduced order model for state estimation the respective simulation times are relevant: the simulation of process using the `LSDyna` model takes 15-20 h while the DMD model requires 70 ms.

3.3 Parametric DMD

A parametric DMD method is the stacked DMD algorithm (Sayadi et al., 2015). This approach is very similar to the non-parametric DMD, except that the time series solutions for different parameter values are "stacked" to form augmented snapshot matrices $X_{1,\boldsymbol{\mu}}$ and $X_{2,\boldsymbol{\mu}}$ in (3). These containing the vertically stacked time series for $N = 7$ parameter realizations $\boldsymbol{\mu} = [\mu_1, \mu_2, \ldots, \mu_N]^T$, which are different process settings for the multi-stage forming process. The stacked matrices are

$$X_{1,\boldsymbol{\mu}} = \begin{bmatrix} X_{1,\mu_1} \\ X_{1,\mu_2} \\ \vdots \\ X_{1,\mu_N} \end{bmatrix}, \; X_{2,\boldsymbol{\mu}} = \begin{bmatrix} X_{2,\mu_1} \\ X_{2,\mu_2} \\ \vdots \\ X_{2,\mu_N} \end{bmatrix}, \; \Phi_{\boldsymbol{\mu}} = \begin{bmatrix} \Phi_{\mu_1} \\ \Phi_{\mu_2} \\ \vdots \\ \Phi_{\mu_N} \end{bmatrix}. \quad (3)$$

The realizations, summarized in Table 1, vary in the process or control variables, respectively, given by the stroke rate f_{SR}, the blank holder force F_{BH}, and the austenitization temperature T_γ. These are subsequently summarized in the tuple $\theta = (f_{\text{SR}}, F_{\text{BH}}, T_\gamma)$, whose elements are supposed to fulfill $6\,/\,\text{min} \leq f_{\text{SR}} \leq 8\,/\,\text{min}$, $5\,\text{kN} \leq F_{\text{BH}} \leq 40\,\text{kN}$, and $1000\,°\text{C} \leq T_\gamma \leq 1100\,°\text{C}$.

The DMD algorithm summarized before is then applied using these matrices of stacked snapshots, which provides the parametric projected DMD modes $\Phi_{\boldsymbol{\mu}}$ from (3). For any new parametric realization θ, the projected DMD modes $\Phi(\theta)$ are obtained from a Lagrangian interpolation between the $\Phi_{\mu,j}$, $j = 1, \ldots, N$ matrices. It is worth mentioning that other interpolation methods are also possible.

Table 1. Parameter sets μ_i for $i = 1, \ldots, N$.

i	f_{SR} in 1/min	F_{BH} in kN	T_γ in °C
1	6	20	1050
2	7	20	1050
3	8	20	1050
4	7	5	1050
5	7	40	1050
6	7	20	1000
7	7	20	1100

For example, the use of Gaussian process regression might be an appropriate choice. The approximate solution for the temperature distribution is

$$\boldsymbol{T}(\theta, t) \approx \Phi(\theta) e^{\Omega t} \boldsymbol{b}(\theta).$$

The different parameter configurations lead to different temperature evolutions. To compare these as results of the parametric DMD, Fig. 5 shows the mean temperature over all nodes $\text{mean}(\boldsymbol{T})$ as a function of f_{SR}, F_{BH} and T_γ at the beginning $t = 0\,\text{s}$ (left) and at the end $t = t_e$ (right) of the forming process. The austenitization temperature T_γ is the only parameter affecting the starting temperature. A higher blank holder force F_{BH} reduces the temperature from the stretch drawing stage. A higher stroke rate f_{SR} accelerates the process leading to higher temperatures at the end of the process.

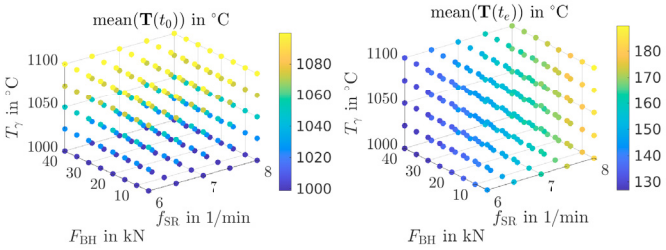

Fig. 5. Temperature evolutions of different parameter configurations for $t_0 = 0\,\text{s}$ and $t_e = 3/f_{\text{SR}}$.

To evaluate the parametric DMD the resulting temperature evolution of four parameter configurations differing from the ones used for the interpolation (cf. Table 1) are compared with the corresponding `LSDyna` simulations. The configuration with $f_{\text{SR}} = 7.5\,/\,\text{min}$, $F_{\text{BH}} = 20\,\text{kN}$, and $T_\gamma = 1050\,°\text{C}$, where the stroke rate f_{SR} differs from the originally used parameter configurations, is depicted in Fig. 6(a). The blue line represents the mean temperature $\text{mean}(\boldsymbol{T})$ simulated with the parametric DMD while grey bars visualize the maximum difference $\max(\Delta\boldsymbol{T})$ between the parametric DMD model and the `LSDyna` simulation at a node and the red bars visualize the mean difference $\text{mean}(\Delta\boldsymbol{T})$ over all nodes. The mean difference is negligible, while the maximum difference is slightly larger especially at the two stage transitions. These results clearly confirm the functionality of the parametric DMD and its high accuracy for extremely low computational times.

Equally good results are obtained for the configuration $f_{\text{SR}} = 7\,/\,\text{min}$, $F_{\text{BH}} = 20\,\text{kN}$, and $T_\gamma = 1025\,°\text{C}$, where the austenitization temperature T_γ differs from the originally used parameter configuration, see Fig. 6(b). Similarly, for configurations with more differing parameters the difference is small as shown for $f_{\text{SR}} = 6.5\,/\,\text{min}$, $F_{\text{BH}} = 30\,\text{kN}$,

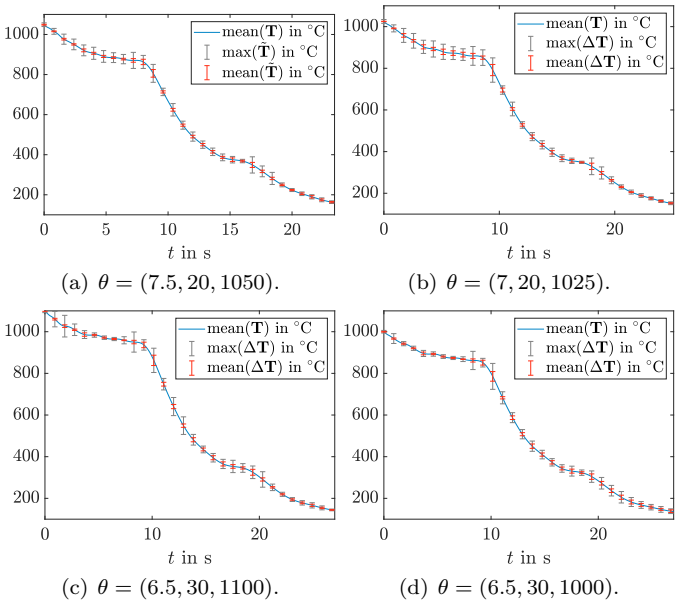

(a) $\theta = (7.5, 20, 1050)$. (b) $\theta = (7, 20, 1025)$.

(c) $\theta = (6.5, 30, 1100)$. (d) $\theta = (6.5, 30, 1000)$.

Fig. 6. Comparison of temperature evolution obtained from parametric DMD with results from an `LSDyna` simulation for different parameter combinations $\theta = (f_{\mathrm{SR}}$ in $1/\,\mathrm{min}, F_{\mathrm{BH}}$ in kN, T_γ in °C).

and $T_\gamma = 1100\,°\mathrm{C}$ in Fig. 6(c) and for $f_{\mathrm{SR}} = 6.5\,/\,\mathrm{min}$, $F_{\mathrm{BH}} = 30\,\mathrm{kN}$, and $T_\gamma = 1000\,°\mathrm{C}$ in Fig. 6(d).

4. DMD-BASED ESTIMATOR DESIGN

The design of an estimator making use of the model generated by parametric DMD is addressed in the following. The main difficulty thereby arises from the fact that the measurements vary in type and location throughout the individual stages eventually leading to a time varying or respectively stage-dependent output matrix.

4.1 Construction of the Output Matrix

The model derived by the parametric DMD combined with the temperature measurements $\boldsymbol{y}(t_k)$ implies the discrete time representation

$$\boldsymbol{T}_r(t_{k+1}) = A_r \boldsymbol{T}_r(t_k), \qquad k \in \mathbb{N}, \quad \boldsymbol{T}_r(t_0) = \boldsymbol{T}_r^0, \tag{4a}$$

$$\boldsymbol{y}(t_k) = C_r(t_k)\boldsymbol{T}_r(t_k), \tag{4b}$$

with $\boldsymbol{T}_r(\cdot) = \boldsymbol{T}_r(\theta, \cdot) \in \mathbb{R}^r$ the reduced state vector and initial values $\boldsymbol{T}_r^0$ at time $t_0 = 0\,\mathrm{s}$. Note that the mapping $\boldsymbol{T}(\theta, t_k) \approx U_r \boldsymbol{T}_r(\theta, t_k) \in \mathbb{R}^n$ approximates the full (nodal) temperature vector. The sampling time $\Delta t = t_{k+1} - t_k = 0.01\,\mathrm{s}$ and the system matrix $A_r(\theta) \in \mathbb{R}^{r\times r}$ are determined by the parametric DMD, while the time varying output matrix $C_r(t_k) \in \mathbb{R}^{n_{\mathrm{sen}}\times r}$ with the number of sensors n_{sen} has to be set up from the actual sensor configuration. As already elaborated in Section 2 the temperature is measured with five spring loaded thermocouples installed in the die stages. Each thermocouple measures the temperature in the sheet blank in one of the three stages while the ram is near the bottom dead center. The temperatures are read with an added thermal imaging camera and pyrometers at these positions, while the press is open. The thermocouple measurements take place at four different locations $p_1 = 12$, $p_2 = 30$, $p_3 = 60$ and $p_4 = 68$ as depicted in Fig. 7 during three simulated stages. In the pre-cooling stage the temperature is measured at two positions p_1 and p_4, in the stretch drawing stage at p_2 and p_3 and in the die bending stage only at p_3.

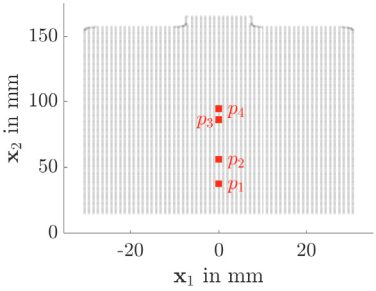

Fig. 7. Measurement positions on the sheet blank.

Consequently the output matrix $C(t_k) \in \mathbb{R}^{n_{\mathrm{sen}}\times n}$ for the full order (non-reduced nodal) system is stage-dependent, which in view of the stroke rate f_{SR} can be transferred to a time varying setting. Let $t_{e,1}$ denote end-time of the pre-cooling stage, $t_{e,2}$ the end-time of the stretch drawing stage, and t_e the process time when passing all simulated stages, the number of rows of $C(t_k)$ is given by

$$n_{\mathrm{sen}} = \begin{cases} 2, & t_k < t_{e,2}, \\ 1, & t_{e,2} < t_k \leq t_e. \end{cases}$$

The respective non-zero elements $C_{i,j}(t_k)$ of $C(t_k)$ can be defined as $C_{1,p_1}(t_k < t_{e,1}) = 1$, $C_{2,p_4}(t_k < t_{e,1}) = 1$, $C_{1,p_3}(t_{e,1} < t_k \leq t_e) = 1$ and $C_{2,p_2}(t_{e,1} < t_k \leq t_{e,2}) = 1$. Applying the projection $C_r(t_k) = C(t_k)U_r$ yields the corresponding output matrix for (4).

4.2 Estimator Design

The estimator is set up in the simulator-corrector form

$$\hat{\boldsymbol{T}}_r(t_{k+1}) = A_r \hat{\boldsymbol{T}}_r(t_k) + L(t_k)\left(\boldsymbol{y}(t_k) - \hat{\boldsymbol{y}}(t_k)\right) \tag{5a}$$

$$\hat{\boldsymbol{T}}_r(t_0) = \hat{\boldsymbol{T}}_r^0, \tag{5b}$$

$$\hat{\boldsymbol{y}}(t_k) = C_r(t_k)\hat{\boldsymbol{T}}_r(t_k) \tag{5c}$$

with $k \in \mathbb{N}$. In particular a discrete time Kalman filter is designed minimizing the variance of the estimation error $\tilde{\boldsymbol{T}}_r(t_k) = \boldsymbol{T}_r(t_k) - \hat{\boldsymbol{T}}_r(t_k)$ under the assumption of zero mean Gaussian process and measurement noise with covariances $Q \in \mathbb{R}^{n\times n}$ and $R(t_k) \in \mathbb{R}^{n_{\mathrm{sen}}\times n_{\mathrm{sen}}}$ (Gelb, 1974).

In the following a comparison between the DMD model $\boldsymbol{T}(t_k)$ and the DMD-based estimator $\hat{\boldsymbol{T}}(t_k)$ is exemplarily evaluated for $\theta = \left(6\,/\,\mathrm{min}, 20\,\mathrm{kN}, 1050\,°\mathrm{C}\right)$. The estimation error $\tilde{\boldsymbol{T}}_r(t_k)$ for an initial value of $\hat{\boldsymbol{T}}_r^0 = \boldsymbol{T}_r^0 + 10\,°\mathrm{C}\,\mathbf{1}$, i.e., an initial deviation of $10\,°\mathrm{C}$ on all states, is depicted in Fig. 8. The average error mean$(\tilde{\boldsymbol{T}})$ over all nodes is small with maximums up to $2\,°\mathrm{C}$ appearing especially at stage changes due to the varying output matrix $C_r(t_k)$, while the maximum error from all nodes max$(\tilde{\boldsymbol{T}})$ is slightly larger within an acceptable range. The error increases after the transition to stretch drawing stage as the used sensor positions change, while it does not increase significantly after the transition to the die bending stage as the processed

sensor is already used in the stretch drawing stage. With this estimator the reconstruction of the spatial-temporal temperature distribution on the sheet metal $\boldsymbol{T}(\theta, t_k)$ is possible for all parameter configurations θ.

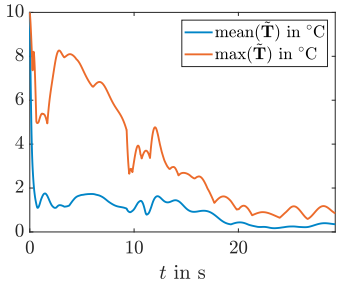

Fig. 8. Mean estimation error over all nodes mean($\tilde{\boldsymbol{T}}$) and maximum error from all nodes max($\tilde{\boldsymbol{T}}$).

5. CONCLUSION

The data-driven temperature estimation for a multi-stage press hardening process with a sheet material in a progressive die is developed and evaluated. Based on data generated by high fidelity FE simulation model realized in `LSDyna` for three subsequent process stages (pre-cooling, stretch-forming, and die bending) a reduced order model is determined using DMD. An extension to a parameter-dependent formulation including the process parameters stroke rate, blank holder force, and austenitization temperature, is proposed to enable the adjustment of the process parameters during estimation and control. It is shown that the simulation results for the parametric DMD model and the original FE model match rather accurately despite the reduction of the computational time from hours to ms. The estimation of the spatial-temporal temperature distribution as a preliminary for property estimation under running conditions is addressed by developing a Kalman filter based on the parametric DMD model. Herein, a time varying or stage-dependent, respectively, output matrix is considered to represent the different number and location of thermocouples in the three stages. Numerical results confirm the applicability of the this designed estimator to reconstruct the temperature profile online. These developments serve as starting point for the realization of a product-property controlled multi-stage forming process.

ACKNOWLEDGEMENTS

The financial support by the Deutsche Forschungsgemeinschaft (DFG) for in the project 424334660 (Tekkaya/ Meurer) within the Priority Program SPP2183 "Property-controlled forming processes" is gratefully acknowledged.

REFERENCES

Allwood, J.M., Duncan, S., Cao, J., Groche, P., Hirt, G., Kinsey, B., Kuboki, T., Liewald, M., Sterzing, A., and Tekkaya, A. (2016). Closed-loop control of product properties in metal forming. *CIRP Annals*, 65(2), 573–596.

Bambach, M., Buhl, J., Hart-Rawung, T., Lechner, M., and Merklein, M. (2017). Towards virtual deformation dilatometry for the design of hot stamping process. *Procedia Engineering*, 207, 1821–1826.

Barocio, E., Pal, B.C., Thornhill, N.F., and Messina, A.R. (2014). A dynamic mode decomposition framework for global power system oscillation analysis. *IEEE Transactions on Power Systems*, 30(6), 2902–2912.

Benner, P., Himpe, C., and Mitchell, T. (2018). On reduced input-output dynamic mode decomposition. *Advances in Computational Mathematics*, 44(6), 1751–1768.

Gelb, A. (1974). *Applied Optimal Estimation*. MIT Press, Cambridge.

Hippchen, P., Lipp, A., Grass, H., Craighero, P., Fleischer, M., and Merklein, M. (2016). Modelling kinetics of phase transformation for the indirect hot stamping process to focus on car body parts with tailored properties. *Journal of Materials Processing Technology*, 228, 59–67.

Hochholdinger, B. (2012). *Simulation des Presshärteprozesses und Vorhersage der mechanischen Bauteileigenschaften nach dem Härten*. Ph.D. thesis, ETH Zurich.

Kloeser, D., Martschin, J., Meurer, T., and Tekkaya, E. (2021). Reduced order modelling for spatial-temporal temperature and property estimation in a multi-stage hot sheet metal forming process. *Advances in Industrial and Manufacturing Engineering*, 3, 100055.

Kutz, J., Brunton, S., Brunton, B., and Proctor, J. (2016). Dynamic mode decomposition: An introduction. In *Dynamic Mode Decomposition: Data-Driven Modeling of Complex Systems*, chapter 1, 1–24. Society for Industrial and Applied Mathematics.

Mamakoukas, G., Abraham, I., and Murphey, T.D. (2020). Learning stable models for prediction and control. *IEEE Trans Robot*.

Mann, J. and Kutz, J.N. (2016). Dynamic mode decomposition for financial trading strategies. *Quantitative Finance*, 16(11), 1643–1655.

Mori, K.i., Maeno, T., Sakagami, M., Ukai, M., and Agatsuma, Y. (2017a). 2-stage progressive-die hot stamping of ultra-high strength steel parts using resistance heating. *Procedia Engineering*, 207, 681–686.

Mori, K.i., Maeno, T., Tsuchiya, M., and Nanya, T. (2017b). Inclusion of hot stamping operations in progressive-die plate forging of tailored high strength gear part. *The International Journal of Advanced Manufacturing Technology*, 90(9), 3585–3594.

Nair, A.G., Strom, B., Brunton, B.W., and Brunton, S.L. (2020). Phase-consistent dynamic mode decomposition from multiple overlapping spatial domains. *Physical Review Fluids*, 5(7), 074702.

Proctor, J.L., Brunton, S.L., and Kutz, J.N. (2016). Dynamic mode decomposition with control. *SIAM Journal on Applied Dynamical Systems*, 15(1), 142–161.

Sayadi, T., Schmid, P.J., Richecoeur, F., and Durox, D. (2015). Parametrized data-driven decomposition for bifurcation analysis, with application to thermo-acoustically unstable systems. *Physics of Fluids*, 27(3), 037102.

Schmid, P.J. (2010). Dynamic mode decomposition of numerical and experimental data. *Journal of Fluid Mechanics*, 656, 5–28.

Shapiro, A. (2009). Finite element modeling of hot stamping. *Steel Research International*, 80(9), 658 – 664.